117

SATELLITE & MESOMETEOROLOGY RESEARCH PROJECT

Department of the Geophysical Sciences
The University of Chicago

OVERSHOOTING THUNDERHEADS OBSERVED FROM ATS AND LEARJET

by

T. Theodore Fujita

SMRP Research Paper
Number 117
January 1974

MESOMETEOROLOGY PROJECT --- RESEARCH PAPERS

1.* Report on the Chicago Tornado of March 4, 1961 - Rodger A. Brown and Tetsuya Fujita

2.* Index to the NSSP Surface Network - Tetsuya Fujita

3.* Outline of a Technique for Precise Rectification of Satellite Cloud Photographs - Tetsuya Fujita

4.* Horizontal Structure of Mountain Winds - Henry A. Brown

5.* An Investigation of Developmental Processes of the Wake Depression Through Excess Pressure Analysis of Nocturnal Showers - Joseph L. Goldman

6.* Precipitation in the 1960 Flagstaff Mesometeorological Network - Kenneth A. Styber

7.** On a Method of Single- and Dual-Image Photogrammetry of Panoramic Aerial Photographs - Tetsuya Fujita

8. A Review of Researches on Analytical Mesometeorology - Tetsuya Fujita

9.* Meteorological Interpretations of Convective Nephsystems Appearing in TIROS Cloud Photographs - Tetsuya Fujita, Toshimitsu Ushijima, William A. Hass, and George T. Dellert, Jr.

10.* Study of the Development of Prefrontal Squall-Systems Using NSSP Network Data - Joseph L. Goldman

11. Analysis of Selected Aircraft Data from NSSP Operation, 1962 - Tetsuya Fujita

12. Study of a Long Condensation Trail Photographed by TIROS I - Toshimitsu Ushijima

13. A Technique for Precise Analysis of Satellite Data; Volume I - Photogrammetry (Published as MSL Report No. 14) - Tetsuya Fujita

14. Investigation of a Summer Jet Stream Using TIROS and Aerological Data - Kozo Ninomiya

15. Outline of a Theory and Examples for Precise Analysis of Satellite Radiation Data - Tetsuya Fujita

16. Preliminary Result of Analysis of the Cumulonimbus Cloud of April 21, 1961 - Tetsuya Fujita and James Arnold

17. A Technique for Precise Analysis of Satellite Photographs - Tetsuya Fujita

18.* Evaluation of Limb Darkening from TIROS III Radiation Data - S.H.H. Larsen, Tetsuya Fujita, and W.L. Fletcher

19. Synoptic Interpretation of TIROS III Measurements of Infrared Radiation - Finn Pedersen and Tetsuya Fujita

20.* TIROS III Measurements of Terrestrial Radiation and Reflected and Scattered Solar Radiation - S.H.H. Larsen, Tetsuya Fujita, and W.L. Fletcher

21. On the Low-level Structure of a Squall Line - Henry A. Brown

22.* Thunderstorms and the Low-level Jet - William D. Bonner

23.* The Mesoanalysis of an Organized Convective System - Henry A. Brown

24. Preliminary Radar and Photogrammetric Study of the Illinois Tornadoes of April 17 and 22, 1963 - Joseph L. Goldman and Tetsuya Fujita

25. Use of TIROS Pictures for Studies of the Internal Structure of Tropical Storms - Tetsuya Fujita with Rectified Pictures from TIROS I Orbit 125, R/O 128 - Toshimitsu Ushijima

26. An Experiment in the Determination of Geostrophic and Isallobaric Winds from NSSP Pressure Data - William Bonner

27. Proposed Mechanism of Hook Echo Formation - Tetsuya Fujita with a Preliminary Mesosynoptic Analysis of Tornado Cyclone Case of May 26, 1963 - Tetsuya Fujita and Robbi Stuhmer

28. The Decaying Stage of Hurricane Anna of July 1961 as Portrayed by TIROS Cloud Photographs and Infrared Radiation from the Top of the Storm - Tetsuya Fujita and James Arnold

29. A Technique for Precise Analysis of Satellite Data, Volume II - Radiation Analysis, Section 6, Fixed-Position Scanning - Tetsuya Fujita

30. Evaluation of Errors in the Graphical Rectification of Satellite Photographs - Tetsuya Fujita

31. Tables of Scan Nadir and Horizontal Angles - William D. Bonner

32. A Simplified Grid Technique for Determining Scan Lines Generated by the TIROS Scanning Radiometer - James E. Arnold

33. A Study of Cumulus Clouds over the Flagstaff Research Network with the Use of U-2 Photographs - Dorothy L. Bradbury and Tetsuya Fujita

34. The Scanning Printer and Its Application to Detailed Analysis of Satellite Radiation Data - Tetsuya Fujita

35. Synoptic Study of Cold Air Outbreak over the Mediterranean using Satellite Photographs and Radiation Data - Aasmund Rabbe and Tetsuya Fujita

36. Accurate Calibration of Doppler Winds for their use in the Computation of Mesoscale Wind Fields - Tetsuya Fujita

37. Proposed Operation of Intrumented Aircraft for Research on Moisture Fronts and Wake Depressions - Tetsuya Fujita and Dorothy L. Bradbury

38. Statistical and Kinematical Properties of the Low-level Jet Stream - William D. Bonner

39. The Illinois Tornadoes of 17 and 22 April 1963 - Joseph L. Goldman

40. Resolution of the Nimbus High Resolution Infrared Radiometer - Tetsuya Fujita and William R. Bandeen

41. On the Determination of the Exchange Coefficients in Convective Clouds - Rodger A. Brown

* Out of Print
** To be published

(Continued on back cover)

OVERSHOOTING THUNDERHEADS OBSERVED FROM ATS AND LEARJET

by

T. Theodore Fujita
The University of Chicago

SMRP Research Paper No. 117

January 1974

Acknowledgements: The successful cloud-truth experiment in 1972 and in 1973 was carried out through excellent team work. The author is grateful to Mr. James Purdom for pinpointing the hot targets as seen in the operational ATS pictures at NSSFC, Kansas City, and to Messrs. Vincent J. Oliver and Edward W. Ferguson for their comments and guidance.

Three meteorologists, Messrs. William Shenk of NASA, Edward Pearl and the author of the University of Chicago, always flew together with the Learjet piloted by Mr. Clyde Alber. The experiment could not have been accomplished without their cooperation.

Overshooting Thunderheads Observed From ATS And Learjet

T. Theodore Fujita

Abstract

Overshooting tops of thunderstorms were photographed simultaneously from both ATS and a Learjet during the cloud-truth experiment over the Midwest in the Spring of 1972 and 1973. The experiment was conducted jointly by the National Aeronautics and Space Administration, the National Environmental Satellite Service, and the University of Chicago.

The characteristics of overshooting tops were studied in various time and space scales, revealing that the horizontal dimensions of overshooting tops vary between 1000 ft and about 10 miles. The period of overshooting turrets with horizontal dimensions of less than 1 mile is found to be comparable to the Brunt-Vaisalla frequency of gravity waves at the lowermost stratosphere. The up-and-down motion of an overshooting dome, consisting of a number of turrets, is much slower than that of individual turrets. We may, thus, assume that the height of a dome is closely related to the intensity of the up and downdrafts beneath the dome. Emphasis is placed upon the importance of the investigation of overshooting domes toward the identification of severe storm characteristics from satellites.

1. INTRODUCTION

Typical thunderstorms in satellite pictures are dominated by fast-spreading anvil clouds. The spreading rates in relation to the severity of storms were investigated

---

The research reported in this paper has been sponsored by the National Oceanic and Atmospheric Administration under grant 04-4-158-1 and by the National Aeronautics and Space Administration under grant NGR 14-001-008.

by Fujita and Bradbury (1969) and by Sikdar, Suomi, and Anderson (1970) based mainly on ATS data. It is natural to conclude that the faster the spreading rate the larger the vertical mass transport into the anvil level. A basic question is, however, the mechanism of the large mass transport which can be accomplished either by a large number of moderate updrafts or a small number of intense updrafts.

The Thunderstorm Project during the years 1946 and 47 revealed the existence of localized updrafts which vary with time. Since a strong updraft is unlikely to stop at the anvil top, the anvil surface may show considerable height variations which are resulted by the spatial and time distribution of the sub-anvil updrafts. Fujita and Byers (1962) presented a model of overshooting hail cloud characterized by a negatively buoyant, cold cloud top.

Newton (1963) produced an overshooting model with an updraft extending into the overshooting top. A few years later, Newton (1966) made a minor revision, so that the cloud materials are transported into the anvil from the overshooting tower. These papers by Newton imply a strong possibility that the sub-anvil updrafts can be estimated from the anvil-top topography.

Horizon-to-horizon pictures taken by U-2 are used by Roach (1966) who proposed a storm-top model. In his model, a cold, overshooting dome is assumed to be supported by a quasi-steady updraft. Roach also considered that the cloud material descending along the side of an overshooting dome spreads into the upper portion of the environmental anvil.

These researches during the 1960s equally suggest the importance of the "overshooting phenomena" characterized by negatively-buoyant protrusions. The protrusion was considered to be in a quasi-steady state by virtue of the existence of a strong updraft which is steady in nature.

Based on radar reports and storm data, Bonner and Kemper (1971) concluded that the tornado probability increases rather slowly with the echo-top height, while the hail frequency shows a significant increase. Their results summarized in Fig. 1 suggest that an extremely high echo-top may not be the prerequisite for tornado formations.

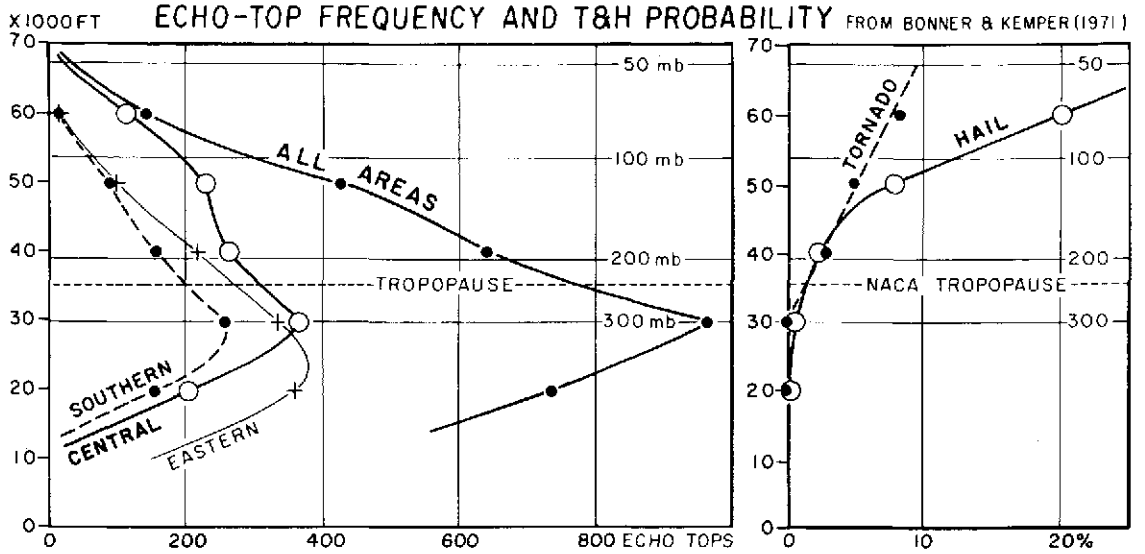

Fig. 1. Frequency of reported radar-echo heights over the U. S. Statistics reveal that the tornado probability does not increase with echo height as much as in the case of hail.

In his study of the spreading rate of ATS-viewed anvils, Purdom (1971) pointed out that tornadoes tend to form when the spreading rate slows down or pauses temporarily. Fujita (1972) made an attempt to compute the height of protrusions above the anvil top, finding that the height decreases 10 to 20 minutes prior to the tornado touch downs. These studies lead to the puzzling characteristics of a suspended anvil growth prior to the development of tornadoes.

Characteristic, 45-min intervals of family tornadoes were found by Fujita (1963). Further investigation of other midwestern tornadoes by Darkow (1971) also revealed that each family tornado is characterized by slightly different occurrence intervals ranging mostly between 40 to 50 minutes. In his radar study of Wisconsin tornadoes on September 16, 1972, Foster (1973) confirmed a periodic formation of 3 tornadoes spawned out of an echo with rotational characteristics. The consistency of the 45-min intervals implies strongly that the periodicity is related to the pulsation of a thunderstorm which produces family tornadoes.

The top of an invisible underwater fountain can be detected as a slight rise of the water surface. If a fountain is strong with its jet-like flow pointing toward the surface, a significant bulge of the water surface will be observed. Likewise, the top of an intense updraft inside a cumulonimbus will appear as a high protrusion.

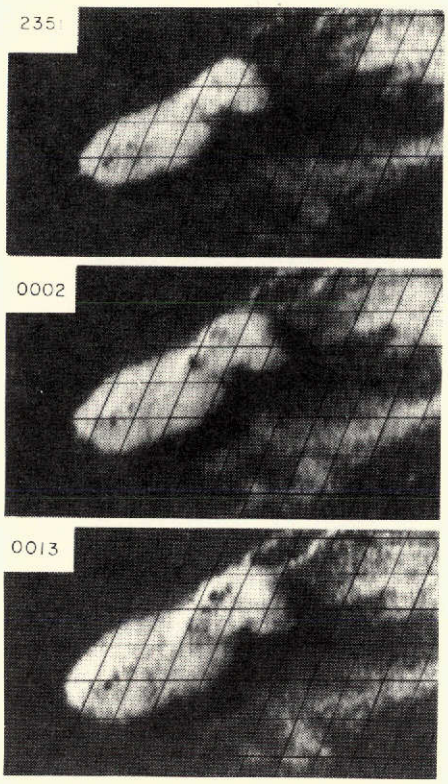

Fig. 2. Fast variations of overshooting domes as seen in a sequence of ATS III pictures. May 11-12, 1970. The cloud was near Salina, Kansas. Geographic grids at 0.5-deg intervals.

Large protrusions are often seen in satellite pictures taken near the terminator. Figure 2 is a sequence of 3 ATS pictures of a thunderstorm taken at 11-min intervals. The dimensions of the most significant protrusion at 0002 are estimated to be 9000 ft high and 10 miles in diameter. As seen in this figure, the shape of protrusions changes rather rapidly. We often find little continuity between pictures.

In an attempt to learn more about the characteristics of protrusions, which signify the tops of intense updrafts as they overshoot into the lower stratosphere, a high-altitude Learjet experiment was conducted. The first cloud-truth experiment was conducted during the tornado season of 1972, followed by a second one in 1973. Since a Learjet with meteorologists on board can travel anywhere in the Midwest, the staging areas were determined daily, by selecting the most probable areas of tornado development.

2. HEIGHT AND PERIOD OF OVERSHOOTING

A fast-rising updraft does not stop at the crossover point, at which the virtual temperature of the rising air coincides with that of the environment. Instead, the vertical motion continues until the kinetic energy decreases to zero at the maximum overshooting height.

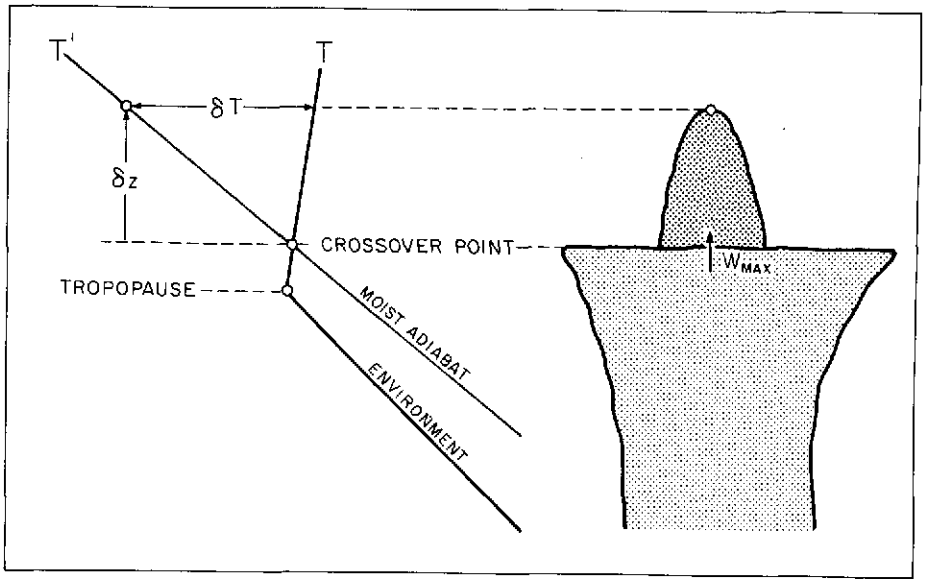

Fig. 3. Schematic diagram showing an overshooting turret. The anvil top is assumed to be at the crossover point. Depending upon updraft intensity, however, the anvil surface could be higher or lower than the crossover point.

With the aid of Fig. 3, the vertical acceleration of the overshooting air can be expressed by

$$\frac{d^2(\delta z)}{dt^2} = -g\,\frac{T-T'}{T} \qquad (1)$$

where δz denotes the overshooting height, T, the environmental temperature, T' the temperature inside the overshooting cloud, and g, the gravity. By using the temperature lapse rates, Γ' and Γ, inside and outside the cloud, Eq. (1) can now be written as

$$\frac{d^2(\delta z)}{dt^2} + K^2\delta z = 0 \qquad (2)$$

$$K^2 = g\,\frac{\Gamma'-\Gamma}{T}$$

where K is a constant applicable to the environment of the overshooting turret. This differential equation is solved as

$$\delta z = \delta z_m \sin Kt \qquad (3)$$

where δz_m is the maximum overshooting height, t the time past the onset of overshooting. The updraft speed can be computed by differentiating Eq. (3), thus

$$W = \frac{d(\delta z)}{dt} = K \delta z_m \cos Kt \qquad (4)$$

which is the largest when $t = 0$, or

$$W_m = K \delta z_m = \delta z_m \sqrt{\frac{g}{T}(\Gamma' - \Gamma)} \qquad (5)$$

where W_m is the updraft speed at the crossover point. The maximum overshooting height can now be expressed by

$$\delta z_m = W_m \sqrt{\frac{T}{g(\Gamma' - \Gamma)}} \, . \qquad (6)$$

The overshooting period is defined as the one-cycle period of Eq. (3). Thus, we write

$$P = \frac{2\pi}{K} = 2\pi \sqrt{\frac{T}{g(\Gamma' - \Gamma)}} \qquad (7)$$

where P is the period of the overshooting cycle. It is evident that the overshooting period is independent of the updraft velocity at the crossover point.

An ideal overshooting cycle may include a series of four motions, which may be identified as rising, collapsing, sinking, and returning motions. Because of strong winds at the tropopause level and of the lack of buoyancy below the crossover point, an overshooting process does not repeat itself, thus lacking the returning motion. Since the sinking motion below the anvil level cannot be confirmed easily, observers get the impression that an overshooting process consists only of rising and collapsing.

If an overshooting motion is sinusoidal, the rising period, as well as the collapsing period, should be one-quarter of the overshooting period, P. Observations revealed, however, that the rising motion could be faster than the collapsing motion or vice versa.

The temperature lapse rate of a moist-adiabat and the air temperature at the tropopause level may be approximated, for most practical purposes, as

$$\Gamma' \cong 9^\circ \text{K/km}$$

$$\text{and } T \cong 200^\circ \text{K}.$$

Using these values and $g = 9.8$ m/sec^2, we are able to tabulate the overshooting period as a function of Γ, the lapse rate within the lowermost stratosphere.

Table I. The total period of overshooting cycle (P), and the rising period (P/4) under the variable environmental lapse rate, Γ.

Γ	-2°	-1°	0°	+1°	+2°	+3°	+4° K/km
P	4.5	4.7	5.0	5.3	5.6	6.1	6.7 min
P/4	67	70	75	79	84	91	100 sec

The table indicates that it will take only about 1 minute for an updraft to overshoot to its maximum level. The negative-buoyancy force is so strong that a rising motion reverses in such a short time. Namely, the natural frequency of the overshooting processes, corresponding to the Brunt-Vaisalla frequency in gravity waves, is so short that a gradual overshooting must be accompanied by an updraft with its period longer than P. In analogy, a pendulum which moves slower than its natural frequency must be under the influence of slow-changing external forces.

Despite the fact that the overshooting period from Eq. (7) is independent of the updraft speed, which reaches a maximum at the crossover point, the maximum overshooting height varies with the updraft speed. Results of computation from Eq. (6) are presented in Table II.

Table II. The maximum updraft speeds required to overshoot into various heights. $\Gamma = 9$°K/km, $T = 200$° K are used. δz_m denotes the maximum overshooting height.

Γ	-2°	-1°	0°	+1°	+2°	+3°	+4°	°K/km
δz_m = 1,000 ft	7.1	6.8	6.4	6.1	5.7	5.2	4.8	m/sec
2,000 ft	14.2	13.5	12.8	12.1	11.3	10.5	9.5	m/sec
3,000 ft	21.3	20.3	19.2	18.2	17.0	15.7	14.3	m/sec
4,000 ft	28.4	27.0	25.7	24.2	22.6	20.9	19.2	m/sec
5,000 ft	35.5	33.8	32.1	30.3	28.3	26.2	23.8	m/sec
10,000 ft	71.0	67.7	64.2	60.5	56.6	52.3	47.7	m/sec

Theoretical considerations based on Brunt-Vaisalla frequency, under the assumption of moist-adiabatic overshooting, reveal that the rising period of an overshooting top should be much shorter than the growth period of tropospheric convective towers.

3. OVERSHOOTING TURRETS

During the cloud-truth experiment in 1972 and 1973, a number of overshooting small turrets 1000 to 3000 ft in diameter were observed from the high-flying Learjet. Time-lapse movies at 1- or 2-second intervals were made to investigate the characteristics of these turrets.

An example of a 2-sec sequence enlarged from super-8 film is shown in Fig. 4. A small turret "A" in the sequence is a typical view of such a turret. A turret usually

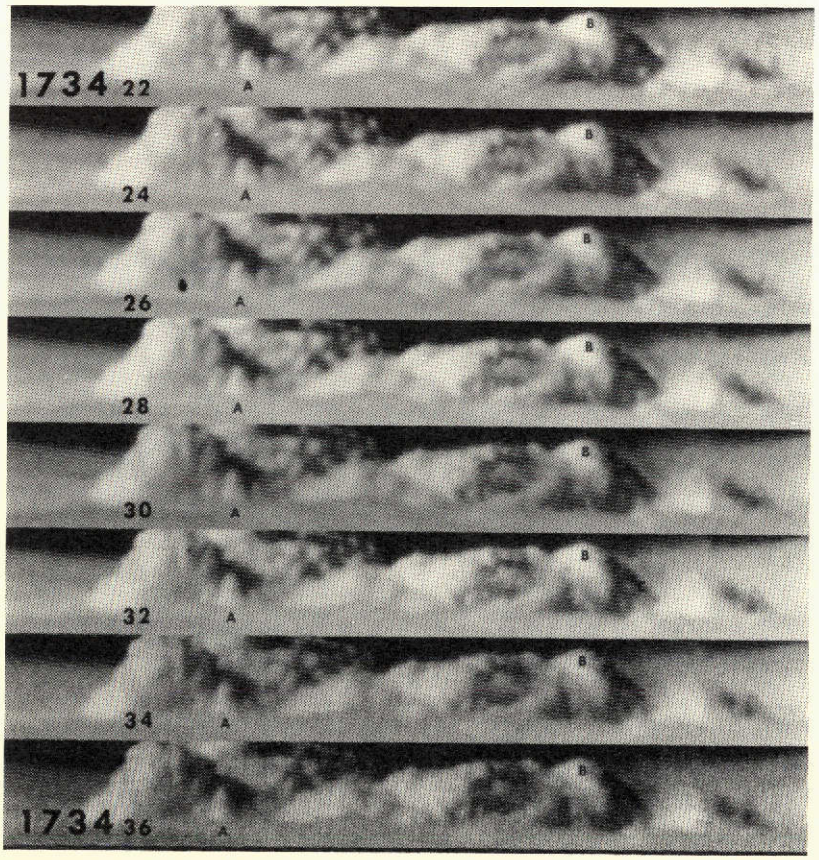

Fig. 4. Fine structure of an overshooting dome filmed at 2-sec intervals. "A" denotes a fast-rising small turret, "B", a large turret, and "C", a small cloud piece sliding down the slope of turret "B". May 12, 1972.

rises very rapidly, reaching its maximum height within an amazingly short time. Thereafter, the top collapses, giving an impression that the whole turret sinks vertically into the sea of anvil cloud.

A number of unexpected phenomena were observed through the Learjet flights at 45,000 ft, occasionally at 50,000 ft to fly over protrusions. While flying under the dark-blue sky, distant protrusions and anvil tops appear to be much higher than our Learjet, giving an impression that we are flying at the bottom of a shallow bowl of high clouds. When we approach a protrusion seen above the visible horizon, the top becomes lower and lower, permitting us to fly over it. When we look back at the top after the flyover, the top is seen above the horizon again. This is because a human tends to estimate the cloud height using the apparent horizon as being the reference. Due to the dip angle, the true horizon is higher than the apparent horizon. A cloud top seen above the apparent horizon could often be located below the true horizon which is invisible. A flight over an active protrusion is mostly turbulent. We often encountered more turbulence slightly on the downwind side where cirrus clouds often extended beyond the flight level. Changes in the overshooting clouds are so rapid that some cloud features could not be identified a few minutes later.

An extremely fast rise, followed by a crushing collapse was the first impression obtained by the three meteorologists, William Shenk, Edward Pearl and the author on board the first Learjet flight in the Spring of 1972.

Shown in Fig. 5 is the variation of the turret top shown in Fig. 4 as a function of time. The maximum turret height and the estimated rising rate at the anvil level were 1760 ft and 18 m/sec, respectively. The lapse rate between 46,000 and 48,000 ft at Brownsville, Texas, 110 n.m. southeast of the cloud, was +4° K/km while at Monterrey, Mexico, 120 n.m. southwest, +2° K/km. If a turret overshoots through a layer of the mean lapse rate of +3° K/km, the maximum overshooting height of 3500 ft will be reached after a 91-sec rising period (refer to Tables I and II).

The maximum overshooting height of turret "A" was 1760 ft, which is just about 50% of the expected overshooting height. Moreover, the rising period of 48 sec in Fig. 5 is only 43% of the period expected from the environmental lapse rate. The storm could, of course, modify the environmental lapse rate. If so, it would require a -10° K/km lapse rate in order to explain the rising period and the height of turret "A". A modification to such an extent would be unrealistic.

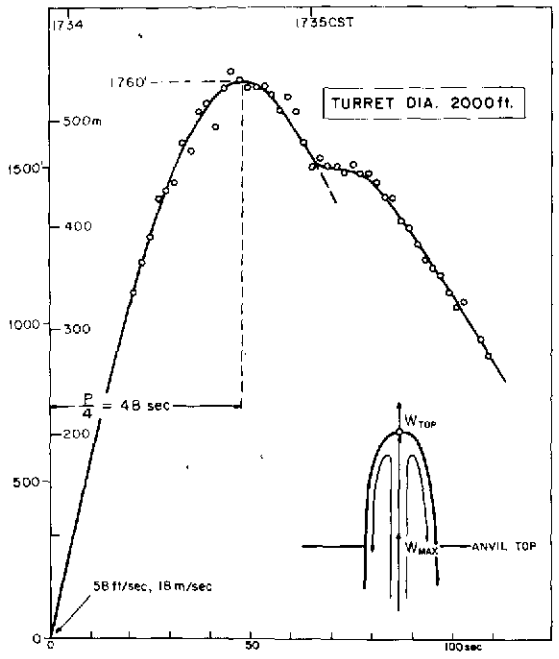

Fig. 5. Time-variation of the overshooting height of turret "A". The rising period was only 48 seconds, with the estimated maximum vertical motion of 18 m/sec. May 12, 1972.

An alternative explanation is the effect of the drag force acting upon the fast-rising air at the turret center. Such a drag force will be created as the adiabatically cooled air descends around a small rising core.

A large turret, up to about one mile in diameter, is quite different from its baby counterpart. A typical example is indicated by letter "B" in Fig. 4. It is seen that a small cloud piece "C" along the turret slope is sliding downslope.

The sliding motion of cloud pieces along the turret slope is presented in Fig. 6. The 3050-ft turret was in its highest stage, while maintaining the steady state for about 30 seconds. The vertical cross section of large overshooting turret, "B" in its steady state is likely to be characterized by a vertical current at the center surrounded by a spreading flow sliding down inside the turret slope.

The variation of the overshooting height of large turret "B" is shown in Fig. 7. During the rising period of 120 seconds, the turret top reached the 3050-ft level above the anvil top. This rising period is not too far from that in Table I, corresponding to +4°K/km lapse rate.

The estimated updraft speed of 14 m/sec and the maximum overshooting height of 3050 ft will also result in about +4°K/km lapse rate in Table II. Therefore, it is

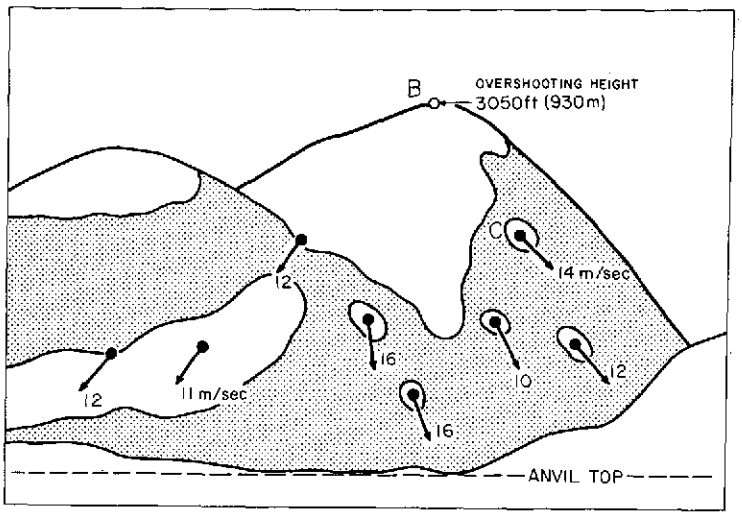

Fig. 6. Small pieces of cloud sliding down the slope of a large turret "B" in its maximum overshooting height. 1734 CST, May 12, 1972.

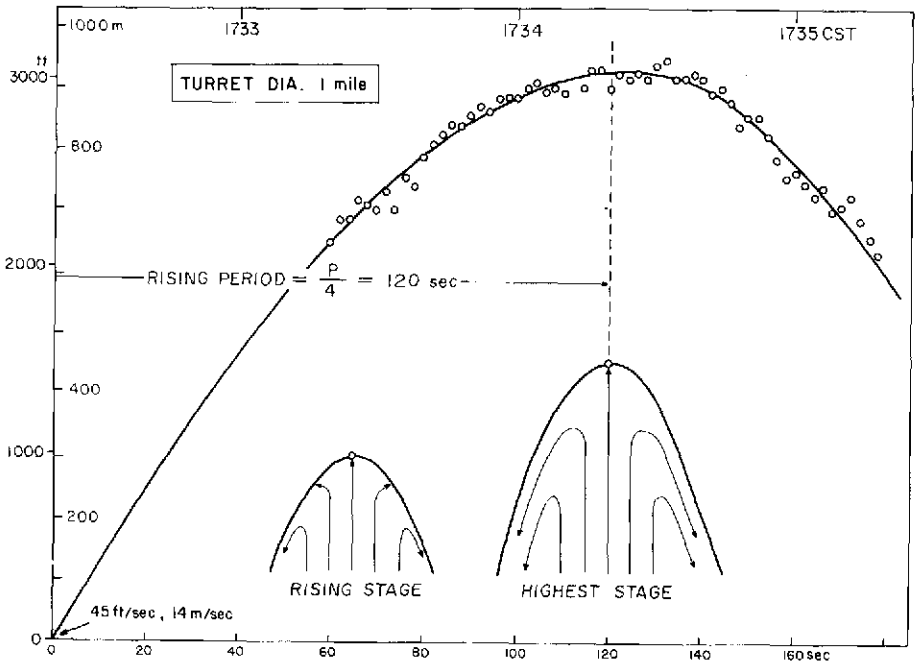

Fig. 7. Time-variation of the overshooting height of large turret "B". The motion of the cloud pieces in Fig. 6 suggests the existence of a rising motion beneath the top in the highest stage. The rising motion will increase the rising period beyond the Brunt-Vaisalla period. 1732-1735 CST, May 12, 1972.

very likely that a large turret overshoots with the Brunt-Vaisalla frequency, suggesting that the drag of the slope current is relatively small. As a result, the rate of rise of the cloud top can be approximated as that of an air parcel being decelerated by the negative buoyancy.

Photogrammetric studies of picture sequences taken at 1 to 2-sec intervals revealed that the above-mentioned characteristics apply to most overshooting turrets, less than about one mile in diameter. These characteristics can be summarized as follows:

1. A large overshooting turret, 0.5 to 1 mile in diameter, overshoots and collapses more or less with the Brunt-Vaisalla frequency shown in Table I. The rising period, which is a quarter of the overshooting period, is usually 1 to 2 minutes.
2. A small overshooting turret, less than 0.5 mile in diameter, reaches its peak height within much shorter time than Brunt-Vaisalla frequency implies. Namely, the rate of deceleration is quite large. Thus, the top starts collapsing prematurely before reaching the overshooting height expected from Eq. (5).

The characteristics of overshooting turrets, less than one mile in diameter strongly suggest that the detection of turrets from geostationary satellite is hopeless from the practical point of view. It is mainly because these turrets change very rapidly. The sum of the rising and the collapsing periods is no more than about 3 to 4 minutes, which is too short to be photographed into a satellite picture sequence.

4. OVERSHOOTING DOMES

A conglomerate of turrets is a common feature prominently seen from a Learjet flying at or just above the anvil level. Individual turrets overshoot and collapse independently, while maintaining the overall features of a conglomerate of turrets which may be called an "overshooting dome" or simply "dome". It should be noted that the terms designating a protrusion are not standardized. Newton (1966) called it a "tower", Roach (1966) a dome, and Shenk (1973) a turret.

The horizontal dimensions of an overshooting dome vary between 1 and 10 miles, consisting of tens to a hundred turrets in various sizes. The dimensions of some domes

are large enough to be detected by ATS sensor with a 2.5-mile resolution at the subpoint. From satellites, it is very difficult to distinguish a dome from its environmental cirrus, because the brightness contrast is very small. It is only the terminator zone where the shadow permits us to visualize the anvil-top topography.

Presented in Fig. 8 is an enlarged ATS picture showing a right-deviating thunderstorm to the south of Lubbock, Texas. The anvil cloud was 100 miles wide and 250 miles long, extending northeastward. No sign of an overshooting dome is visible in the ATS picture because the anvil top is bright.

From a distance of about 250 miles, while flying toward the cloud we found a large dome on the southwest side of the anvil cloud. As we approached the distance of about 100 miles, the structure of the dome became apparent. A sequence of telephoto

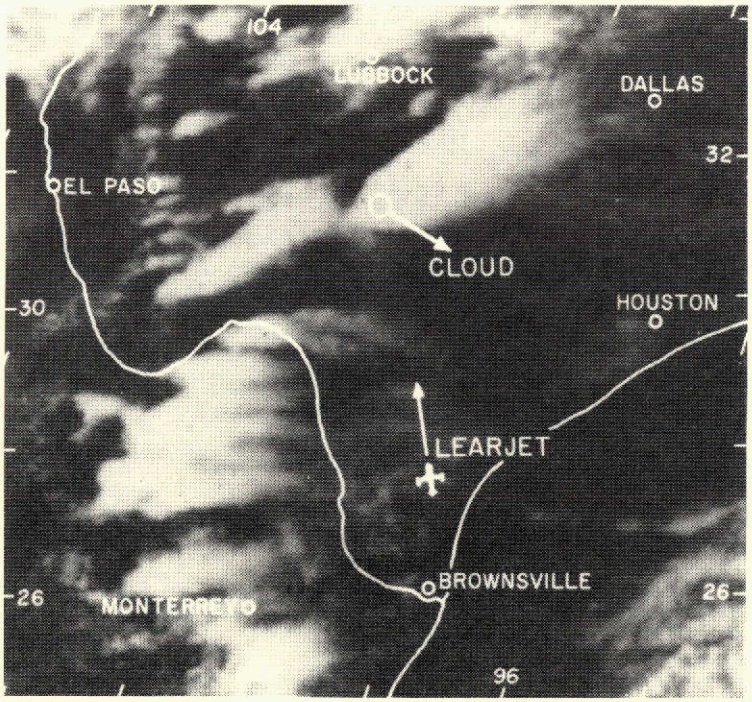

Fig. 8. Investigation of a right-deviating cloud by a Learjet. Overshooting tops are not visible in this ATS picture taken at 1537 CST, May 13, 1972.

pictures taken at 1-min intervals are shown in Fig. 9. The picture covers a west (left) to east distance of about 12 miles. The height of the dome was about 3000 ft.

The anvil top was so flat that the overshooting dome looked very much like the islands floating on a sea of anvil cloud. Individual turrets in the dome were rising and

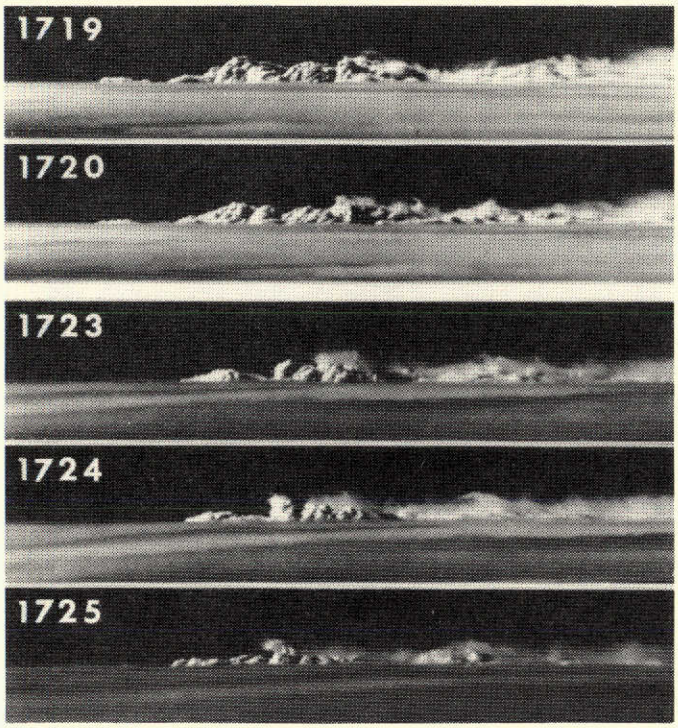

Fig. 9. Telephoto view of the right-deviating cloud in Fig. 8 taken from a Learjet flying 100 miles away from the cloud. May 13, 1972.

sinking as if they were giant buoys.

It may sound strange, however, the surface of the anvil top was flat, without being influenced by the up and down motions of individual turrets. At first, we expected to see a slight bulge of the anvil surface surrounding a rising turret. We looked also for a rise in the anvil surface on the upwind side of the dome. Despite the fact that the environmental wind at the anvil level was 89 kt from the due west and the radar echo motion was only 30 kt from the 300° direction, the anvil surface was perfectly flat.

Similar phenomena were confirmed throughout the Learjet flights in 1972 and 73, suggesting strongly the existence of a significant stability characterized by a well-defined tropopause. A proposed mechanism of the formation of such a tropopause will be discussed later.

Variation of an overshooting dome during a 2-min period is shown in Fig. 10. This is a typical dome frequently observed during the experiment. Some turrets within the dome are identifiable but others are not. It will be seen, however, that the dome consists of a number of turrets in various stages of overshooting.

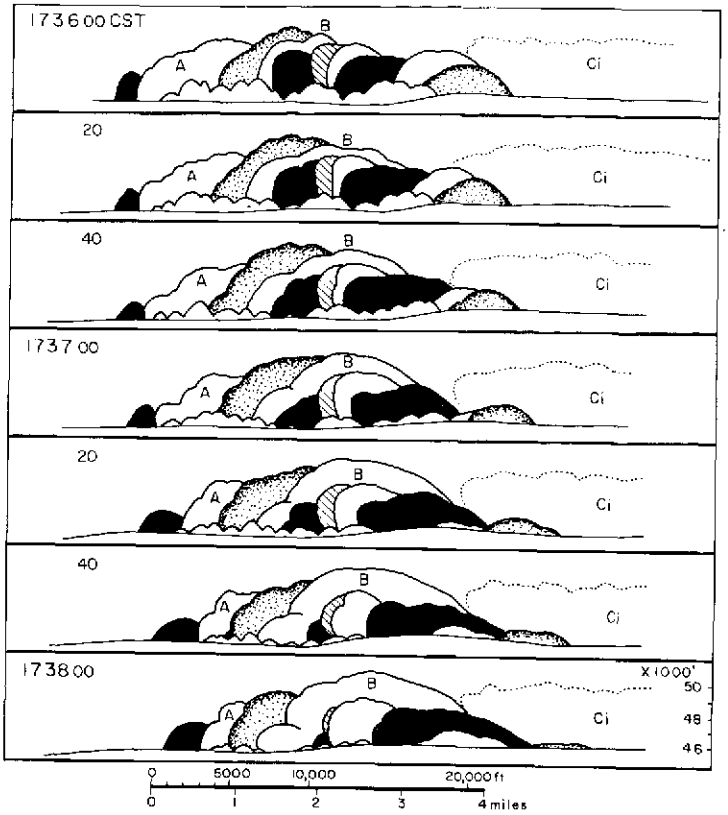

Fig. 10. An overshooting dome of May 12, 1972, consisting of a number of turrets in various overshooting stages.

The variations of the dome top were measured at 2-sec intervals to determine the overall changes in the dome height. A result in Fig. 11 clearly indicates that the height variation involves two scales of motion. The one, comparable to the Brunt-Vaisalla frequency and the other, corresponding probably to the oscillation of the dome-scale updraft underneath.

The overshooting period of a dome shows a wide variation. Shenk (1973), a co-investigator, measured the height variations of 21 domes to obtain a statistical variation of the dome height. Shenk's statistics revealed the averaged rising period of about 5 minutes, which corresponds to the overshooting cycle of 20 minutes.

The Byers-Braham (1949) model resulting from the Thunderstorm Project in 1946-47 is characterized by the transition of updraft into downdraft due to the precipitation loading. Hydrometeors in their model are assumed to fall into the updraft, thus

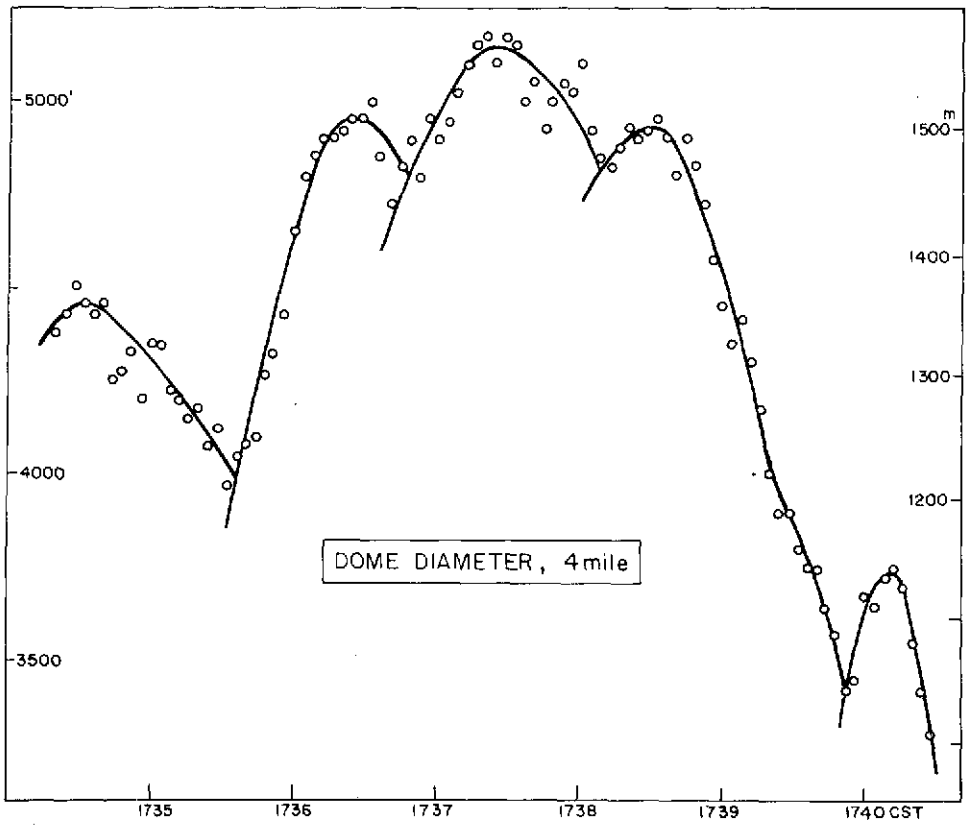

Fig. 11. Variation of the overshooting height of a dome, 4 miles in diameter. Four Brunt-Vaisalla frequencies are superimposed. May 12, 1972.

reducing the draft speed to zero, finally reversing the flow direction to generate a downdraft. The period between the formation of successive updrafts was estimated to be 15 to 20 minutes.

For about a decade, the concept of a steady-state model by Browning and Ludlam (1962) was utilized to explain the circulation of severe storms. In order to avoid the precipitation overloading, a concept of sloped updraft was introduced. Now, a major problem is the definition of "steady state". Regardless of the updraft variation, the state of a flow may be considered steady when a maximum value is reached, say, at $t = t_0$. Shortly after the maximum, the local derivative will change into

$$\left(\frac{\delta}{\delta t}\right)_{t_0+dt} = \left(\frac{\delta}{\delta t}\right)_{t_0} + \frac{\delta^2}{\delta t^2} dt \ . \qquad (8)$$

If we define a semi-steady-state when

$$(\lambda) = \left(\frac{\delta}{\delta t}\right) / \left(\frac{\delta}{\delta t}\right)_{MAX} \qquad (9)$$

is very small, an oscillating updraft may be regarded as semi-steady-state for a short period of time. In order to estimate the period of such a semi-steady-state, we assume a sinusoidal oscillation expressed by

$$\delta z = \delta z_m \sin \frac{2\pi t}{P} \qquad (10)$$

where P denotes the overshooting period. A combination of Eqs. (8) and (9) permits us to write

$$\pm \lambda = \frac{\delta^2}{\delta t^2} \Delta t / \left(\frac{\delta}{\delta t}\right)_{MAX}$$

$$= \frac{-\frac{4\pi^2}{P^2} \Delta t \sin \left(\frac{2\pi t}{P}\right)_{t=\frac{P}{4}}}{\frac{2\pi}{P} \cos \left(\frac{2\pi t}{P}\right)_{t=0}}$$

$$= -\frac{2\pi}{P} \Delta t \qquad (11)$$

where Δt is the half-period of the assumed semi-steady-state. The total period, $2\Delta t$ is now expressed by

$$2\Delta t = \frac{\lambda P}{\pi} \quad . \qquad (12)$$

If we consider that $\lambda = 0.1$ is acceptable for the semi-steady-state, the period can be approximated as

$$2\Delta t \cong 0.03P \quad . \qquad (13)$$

The semi-steady-state period of an overshooting turret from Eq. (13) and Table I is only about 10 seconds. For Shenk's overshooting dome with a 20-min period, the semi-steady-state period appears to be only about 40 sec. So far, we have failed to locate long-lasting overshooting dome likely to be found above a hypothetical steady-state updraft.

Kessler's (1971) numerical model, involving a vertical, time-dependent, moist convection, suggests possibilities of updraft oscillation. The periods of damped oscillation were computed to show their wide range of variations, ranging from 30 min to that of a steady state. Since his probable oscillation periods are considerably longer

than the natural frequency of the overshooting turrets, the intensity, mode, and period of the updraft oscillation are very likely to be estimated from the characteristics of overshooting turrets and domes.

5. PROPOSED MECHANISM OF TROPOPAUSE MODIFICATION BY THUNDERSTORMS

The existence of an outflow field at the top levels of a thunderstorm was pointed out by a number of authors. McLean's (1961) study of Doppler winds during the Project Jet Stream confirmed a significant outflow from the top of a localized squall line over Bryan, Texas. There are a number of cases in which the jet-level divergence was increased by the presence of thunderstorms.

Since ATS pictures became available, a number of researchers have computed upper divergence field by tracking anvil boundaries or by computing high-cloud velocities. Refer to Fujita and Bradbury (1969), Sikdar et al. (1970), Purdom (1971), and many others.

These studies provide us with convincing evidence pertaining to a localized high-pressure field at the tropopause level. Close-up views of ATS pictures in a time-lapse loop often reveal an upwind growth of the edge of an expanding anvil. An example of expanding anvils, A and B, is shown in Fig. 12. The boundaries were obtained from 2/5-scan pictures taken at about 11-min intervals.

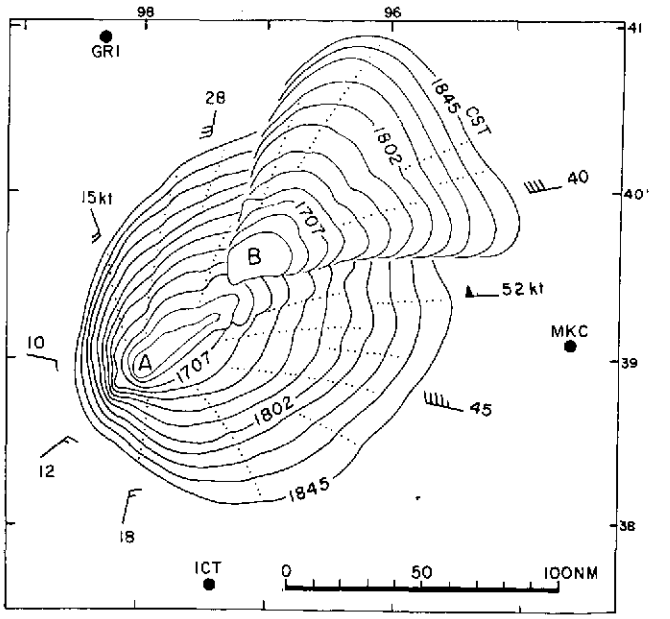

Fig. 12. An example of an expanding anvil obtained by combining 12 ATS pictures taken at 11-min intervals on May 11, 1970. Dotted lines denote the motion of cloud elements at the anvil edges. The anvil-level wind was 255° - 39kt.

It is evident that the southwest edge of anvil A expanded upwind at 10 kt while the 200-mb wind was 39 kt from the 255°, the direction of the gradient wind. The anvil growth was not symmetric, expanding toward the left and the right of the general flow direction. Especially, the right-side growth cannot be achieved unless the storm produces a mesoscale high-pressure field strong enough to offset the large-scale pressure gradient.

Anvil B was under the influence of A, thus restricting its growth in the directions opposite from the action center of A. Of interest are the trajectories of anvil materials obtained by connecting corresponding minor features on successive anvil boundaries. With the scale of this anvil, the trajectories show a slight anticyclonic curvature.

The rotational speed of the earth, V_E as viewed from the spreading center is

$$V_E = \frac{1}{2} fR \qquad (14)$$

where f is the Coriolis parameter, R the distance from the spreading center. If we assume that $f = 10^{-4}\ sec^{-1}$, the rotational speeds are 1 m/sec at the 10 km radius and 10 m/sec at 100 km. The order of magnitude of the estimated tangential speed suggests that anticyclonic features of anvil expansion will become visible when the spreading distance exceeds 100 km or about 50 miles.

In an attempt to clarify the mechanism of the anvil-cloud spreading, edges of anvils were photographed from Learjet flying at the anvil altitude. As shown in Fig. 13, a very thin edge often extends upwind. The edge gives an impression that the uppermost anvil is sliding out with a small curl along the edge.

Several times we witnessed cloud vortices as shown in Fig. 14. These vortices are located away from the upwind-side edge, hanging in the free atmosphere. These two views give a definite impression that the clear air above the anvil top is spreading out faster than the underlying anvil materials.

The proposed flow patterns of a spreading anvil cloud are presented in Fig. 15. The moist adiabat of the updraft intersects the temperature of the far environment at the crossover point, the height of natural stability. If the anvil top is pushed upward by the overall rising motion of the in-cloud air, the anvil-top temperature will decrease several degrees until reaching the height of equilibrium. The atmosphere directly

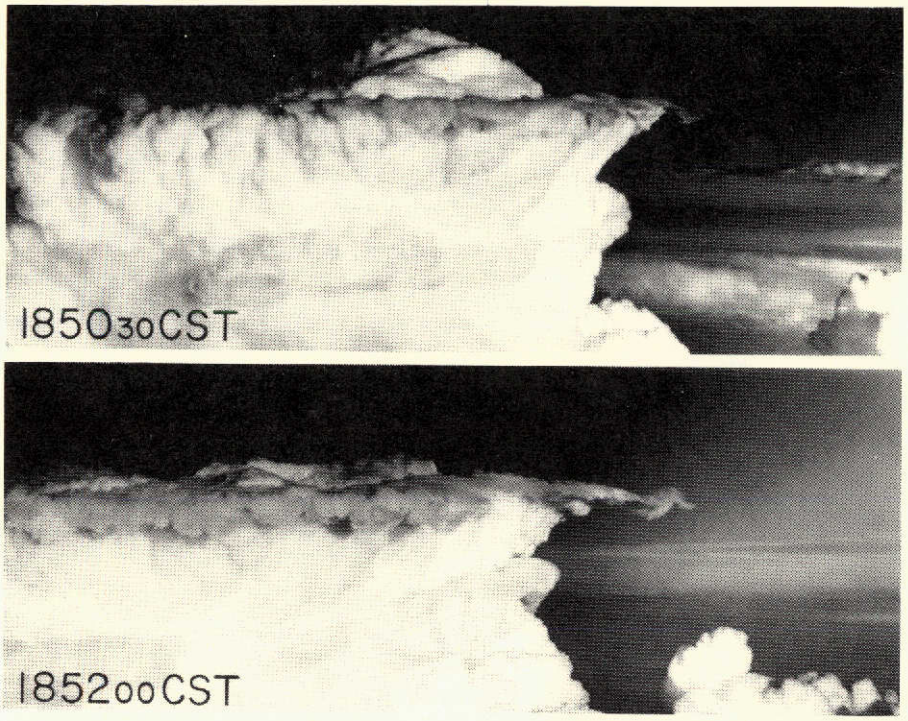

Fig. 13. The skin of an anvil surface spreading outward. Pictures were taken looking south, while the anvil level wind was 97 kt from the west. Note that the spreading motion intensified when the turret collapsed in 90 seconds. May 6, 1973.

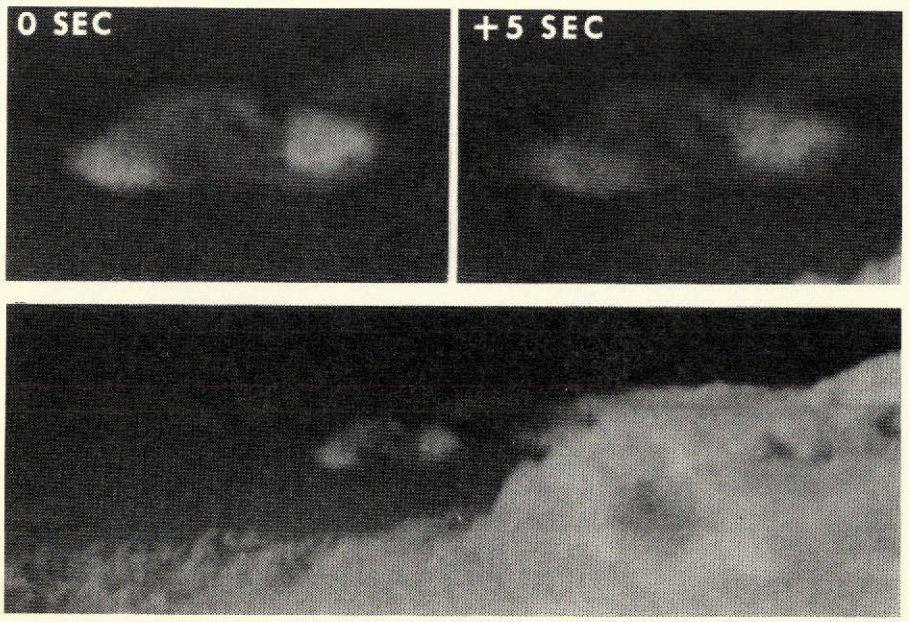

Fig. 14. Smoke rings emerging out from the anvil top near the Mexican border on May 12, 1972. These rings were seen on the west side when the 200-mb wind over Monterrey was 100 kt from the west.

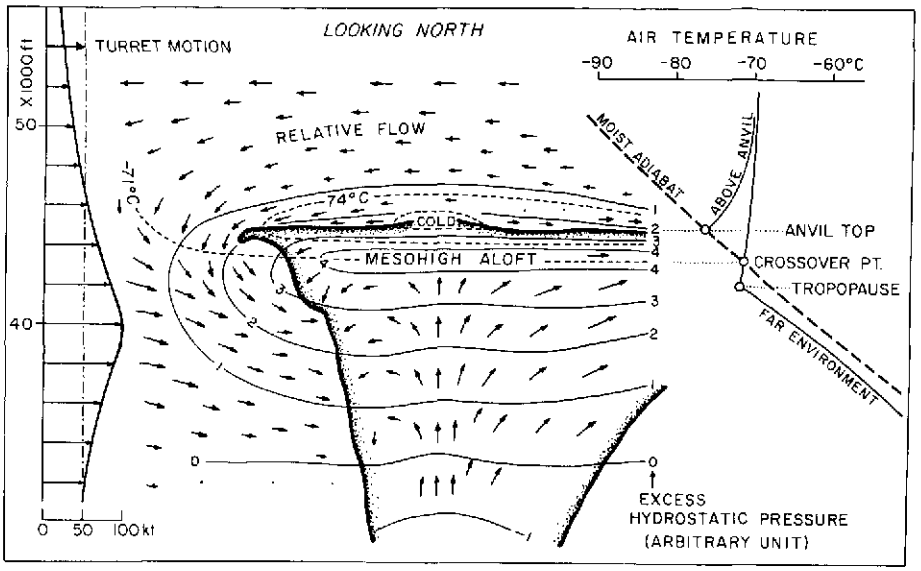

Fig. 15. A model of mesohigh aloft accompanied by the horizontal pressure gradient to shield the jet-level winds blowing toward an anvil cloud. Arrows indicate the flow relative to overshooting turrets. The cold-air outflow just above the anvil surface pushes the anvil skin to generate a curl or ring vortex at or near the anvil edge.

above the anvil is also pushed upward, while diverging outward beyond the anvil edge. Thus, the anvil cloud above the crossover point is colder than the environment. Moreover, a blanket of cold air covers the cold top of the anvil. The total thickness of the cold air, extending upward from the crossover point, is likely to be several thousand feet.

The hydrostatic pressure inside this cold air is naturally higher than the environment, reaching the maximum at the level of the crossover point. A field of excess pressure somewhat like that of a mesohigh on the ground will be found near the anvil-top level. The high-level mesohigh produced by an anvil may be called the "Mesohigh Aloft". The altitude of a mesohigh aloft is higher than the tropopause at the undisturbed environment. Thus, a lifted tropopause forms at the anvil-top level. It is the lower stratospheric air which diverges out above the anvil top to descend from around the edge.

The horizontal pressure gradient of the mesohigh aloft provides the outward acceleration of both anvil cloud and the overriding stratospheric air. By virtue of the horizontal spreading of the cold air above the crossover point, the mesohigh aloft

extends beyond the edge of a spreading anvil, thus acting as a protective shield with anvil cloud inside.

One of the engines of our Learjet, in a photographic mission on May 12, 1972, suddenly quit while flying at about 50,000 ft, overlooking the Rio Grande near Brownsville. All of us were breathing oxygen at this altitude. Our pilot decided to dive down to about 20,000 ft as quickly as possible before the other one might also quit, resulting in the loss of the cabin pressure. Fortunately, nothing happened except that a tiny, snake-like Rio Grande changed into a big river within a very short time.

Just about 10 minutes before the engine quit, the pilot had asked us why the outside air temperature was extremely low. It was -84° C or 189° K which was the coldest he had ever experienced over the Midwest. Since we were busy in taking pictures, none of the three meteorologists paid attention to the pilot's question on the cold temperature until the engine failed to function due to "gas-line freeze".

The anvil top at about 42,000 ft gradually increased its surface to 45,000 ft, further to 49,000 ft toward the unexpected termination of the experiment at 1746 CST. At that time we could barely see the foot of overshooting domes from about 50,000 ft.

The temperature of the anvil surface will decrease 3° C per 1000-ft lifting, or 9° K/km, without counting the radiative heat loss. A 7000-ft lifting of the anvil during the mission would have dropped the anvil-surface temperature by 21° C. It is our belief that we were flying inside an extremely cold mesohigh aloft when one of the fuel lines froze.

We have, ever after, been avoiding the flight inside an extremely cold mesohigh aloft. Several attempts were made to fly over the domes extending up to a 50,000-ft altitude. However, an extremely low temperature has not been encountered during these overflights, because the mesohigh aloft did not extend to our altitude. It is very likely that the stratospheric air above an overshooting dome simply slides down the dome slope, without being lifted adiabatically.

6. FLOW ABOVE THE ANVIL TOP AND STRATOSPHERIC CIRRUS

Most of the photographic missions in 1972-73 tornado seasons were made over the central and southern Midwest when jet-level winds were about 100 kt. At the dome-top levels between 45 and 52,000 ft, the stratospheric winds were predominantly westerlies with 50 to 70-kt speeds.

There were considerable cirrus clouds in the stratosphere above relatively old anvil clouds with active domes. Fly-by observations revealed that the stratospheric cirrus clouds originate when overshooting turrets or domes collapse rather rapidly. During such a collapsing stage, cirrus clouds literally jump up 5,000 to 10,000 ft beyond the anvil surface.

Shown in Fig. 16 are three pictures showing the "jumping motion" of the stratospheric cirrus. A long trail of cirrus extending to the right (east) edge of the pictures are the old cirrus produced by the domes and turrets which had already collapsed.

The top of the stratospheric cirrus at about 50,000 ft was under the influence of, say, 50 kt westerlies. The time-motion analysis revealed, however, that the cirrus moves toward the turrets located to the west of the cirrus front. As seen in the example, protrusions are often overtaken by the approaching cirrus, thus disappearing into the cloud. We often got an impression that an advancing cirrus front chases protrusions until they are swallowed by the cloud.

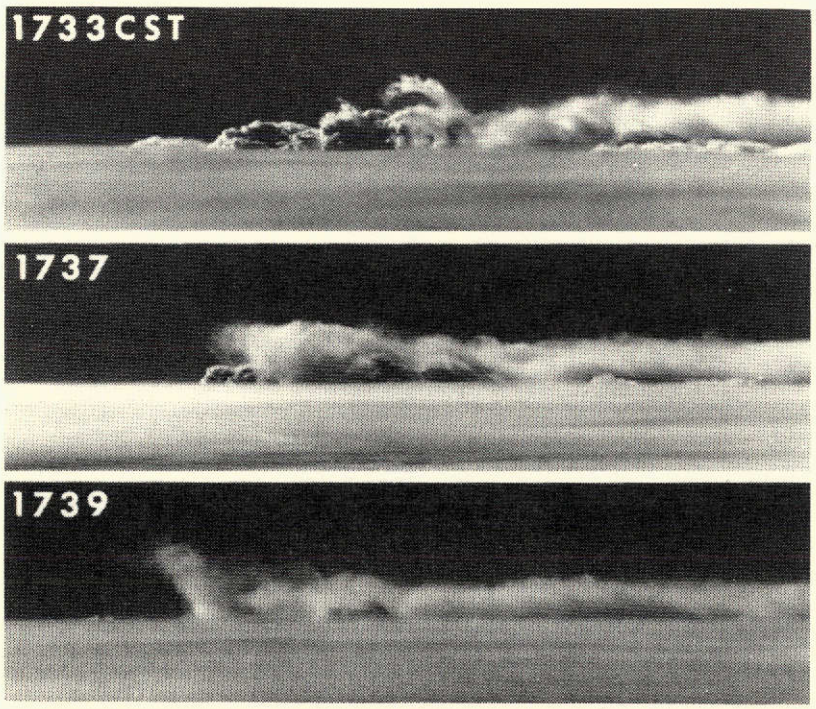

Fig. 16. Lower stratospheric cirrus, the turret eater. Acting as a long-tailed dragon, a large mass of cirrus swallows overshooting turrets and domes. A Learjet view of this phenomenon is spectacular. May 13, 1972. Pictures looking north.

A definite reversal shear is seen within the entire cirrus layer above the anvil top. Relative to the anvil surface, the cirrus top usually moves 20 to 30 kt westward indicating the vertical wind shear of about 6 kt per 1000 ft or 10 m/sec per km.

The fact that the stratospheric cirrus, moving westward at about 50 kt, overtakes protrusions leads to a conclusion that overshooting turrets must be moving eastward faster than 50 kt. Otherwise, the stratospheric cirrus cannot approach the turrets from the east.

A collapsing turret shown in Fig. 17 was analyzed by using a time-lapse sequence taken at 1-sec intervals. To our surprise, the east wall of the turret was sinking at the rate of 41 m/sec. The velocity vectors represent the motion relative to the turret center. The stratospheric cirrus was approaching from the east. Fortunately there was a narrow cirrus-free space, permitting the computations of the sinking velocities of tiny cloud elements. After observing this phenomenon shortly after 1700 CST, the cloud top was monitored for about 1-1/2 hours until 1830 CST when we had to leave the area for refueling.

Fig. 17. A collapsing turret, being chased by the stratospheric cirrus to the left (east). The east wall of the turret is sinking at 41 m/sec.

A model of a collapsing dome with new stratospheric cirrus clouds is presented in Fig. 18. Vectors in the model circulation represent the motion relative to the turret moving eastward at about 50 kt. The motion of the stratospheric cirrus is such that the collapsing features of a turret is mostly covered with a mixture of new and old cirrus

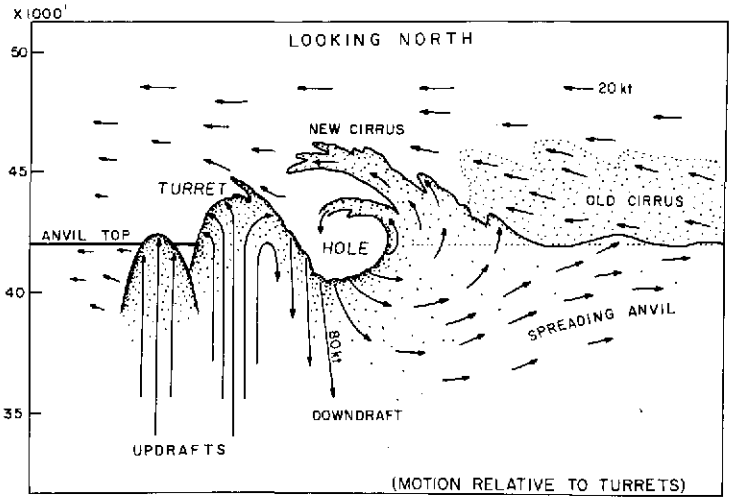

Fig. 18. A model circulation of a fast-collapsing turret. Our Learjet encountered moderate to severe turbulence while flying over a collapsing turret. No flight over a hole has been attempted. An approach to the fast-sinking wall is risky.

clouds. Evidence of fast sinking motions of collapsing turrets suggests the existence of a deep hole on the anvil top. An oblique photograph of such a hole has not been made from a Learjet, because we do not feel safe to fly over the hole topped by a new cirrus moving violently toward the east wall of a collapsing turret. Time-lapse movie made from a series of horizontal pictures gives an impression that a Learjet could be swept into the hole if we attempt to fly through it.

Despite the evidence that the overshooting turrets move at the rate of 50 kt or even faster, the motion of the corresponding echo is only 20 to 30 mph. Why do echoes move much slower than individual turrets?

Examination of cloud pictures taken at 15 to 30-sec intervals revealed that new turrets have a tendency to form on the west or southwest side of collapsing ones. This tendency will slow down the motion of a dome consisting of a number of turrets.

A schematic distribution of the vertical velocity at the anvil-top level is presented in an x-t diagram of Fig. 19. It is seen that the individual turrets with a relatively short life of several minutes move from west to east at 60 kt. New turrets keep forming on the west side so that the overall motion of the dome or a group of turrets propagates slower than turrets. The overall location of the downdraft should be comparable to

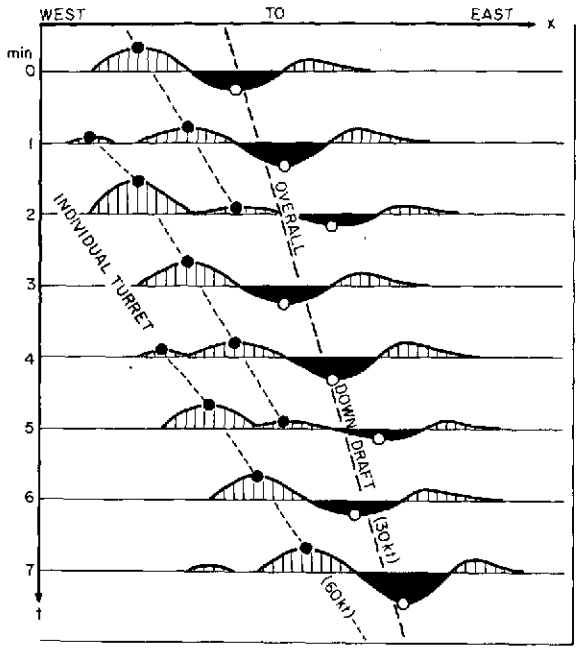

Fig. 19. A x-t diagram showing that an individual turret can move faster than the overall downdraft region. Both time and space integration of downdrafts at the anvil level will result in a precipitation cell at lower levels.

that of a dome rather than a turret. Thus, a precipitation cell or the thunderstorm echo to be located beneath the anvil-level downdraft has a tendency to move slower than the overshooting turrets aloft.

7. CONCLUSIONS

The cloud-truth experiment during the 1972 and the 1973 tornado seasons clarified the characteristics of turrets and domes overshooting into the lower stratosphere. Most turrets are less than one mile in diameter with an overshooting period of only a few minutes. It is, therefore, impractical to attempt to detect these turrets by means of meteorological satellites.

On the other hand, overshooting domes are as large as several to ten miles in diameter while overshooting much slower than turrets. Learjet photographs of various domes suggest strongly that their overshooting activities are closely related to the variation of draft velocities beneath the anvil surface. Once the relationship between draft velocities and the nature of severe storms becomes well established, it is likely that we will be able to infer severe-storm types based on the satellite-observed overshooting domes.

The following relationships, hypothetical in nature, have been suggested for possible confirmation through an expanded cloud-truth experiment within the next few years.

(A) HAILSTORMS. Bonner and Kemper's (1971) statistics and other evidence reveal that the hail probability increases with the echo-top height. It is likely that hailstorms can be monitored by satellite, based mainly on the height and temperature of overshooting domes.

(B) TORNADO CYCLONES. The 45-min frequency of family tornadoes confirmed by Fujita (1963) and Darkow (1971) suggests a possible variation of the overshooting dome with the 45-min period. Fujita (1973) proposed that the tornado occurrence takes place during the downdraft stage of a rotating thunderstorm. It is proposed that a tornado cyclone as well as the tornado occurrences can be monitored based on the overshooting frequency and the deviation of the dome motion.

(C) ORDINARY THUNDERSTORMS. Byers-Braham type thunderstorms are likely to be characterized by a 15 to 20-min period. The overshooting domes of these thunderstorms are likely to change with such a pumping period. The overshooting heights will be moderate.

(D) RAINSTORMS. Rainstorms are not characterized by intense updraft. Insignificant overshooting coupled with relatively slow oscillation appears to be the characteristics of rainstorms.

The main objectives of future cloud-truth experiments are to relate "what is seen from above" with "what takes place on the ground". Both theoretical and statistical knowledge, to be accumulated through such an experiment, can be used for the improvement of nowcasting and forecasting severe weather phenomena.

Additional information such as 3-dimensional radar, upper-air and surface network data, ground photography of storm clouds and tornadoes, cooperative observations of all types, etc. are of vital importance to the experiment, if they are available at the time and location of the severe storm event to be investigated.

References

Bonner, W. D. and J. E. Kemper (1971): Broad-scale Relation between Radar and Severe Weather Reports. 7th Conf. on Severe Local Storms, Kansas City, pp 140-147.

Browning, K. A. and F. H. Ludlam (1962): Airflow in Convective Storms. Quart. J. Royal Met. Soc., 88, 117-135.

Byers, H. R. and R. R. Braham (1949): The Thunderstorm. U. S. Government Printing Office, Washington, D. C. 287 pp.

Darkow, G. L. (1971): Periodic Tornado Production by long-lived Parent Thunderstorms. 7th Conf. on Severe Local Storms, Kansas City, pp 214-217.

Foster, H. (1973): Tornado Echo Study with "VIP". 8th Conf. on Severe Local Storms, Denver, pp 161-164.

Fujita, T. T. and H. R. Byers (1962): Model of Hail Cloud as revealed by Photogrammetric Analysis. NUBILA, 1, 85-105.

Fujita, T. T. (1963): Analytical Mesometeorology: A Review. AMS Meteorological Monograph Vol. 5, No. 27, 77-125.

Fujita, T. T. and D. L. Bradbury (1969): Determination of Mass Outflow from a Thunderstorm Complex using ATS-III Pictures. 6th Conf. on Severe Local Storms, Chicago, 38-43.

Fujita, T. T. (1972): Tornado Occurrences related to Overshooting Cloud-top Heights as determined from ATS Pictures. SMRP Res. Paper 97, 32 pp.

Fujita, T. T. (1973): Proposed Mechanism of Tornado Formation from Rotating Thunderstorm. 8th Conf. on Severe Local Storms, 191-196.

Kessler, E. (1971): Model of Precipitation and Vertical Air Currents. NOAA Tech. Memo. ERL NSSL-54, 93 pp.

McLean, G. S. (1961): Observation of Severe Convective Activity in a Squall Line. Bull. Amer. Met. Soc., 252-264.

Newton, C. W. (1963): Dynamics of Severe Convective Storms. AMS Meteorological Monograph Vol. 5, No. 27, 33-58.

Newton, C. W. (1966): Circulation in Large Sheared Cumulonimbus. Tellus XVIII, 4, 699-712.

Purdom, J. F. W. (1971): Satellite Imagery and Severe Weather Warning. 7th Conf. on Severe Local Storms, Kansas City, 120-127.

Roach, W. T. (1966): An Analysis of Eight Flights by U-2 Aircraft over Severe Storms in Oklahoma. Tech. Memo ERTM-NSSL-29, 23-52.

Shenk, W. (1973): Cloud top height variations of Strong Convective Cells. 8th Conf. on Severe Local Storms, 80-83.

Sikdar, D. N., V. E. Suomi and C. E. Anderson (1970): Convective transport of mass and energy in severe storms over the United States--an estimate from a geostationary altitude. Tellus XXII, 5, 521-532.

MESOMETEOROLOGY PROJECT - - - RESEARCH PAPERS

(Continued from front cover)

42.* A Study of Factors Contributing to Dissipation of Energy in a Developing Cumulonimbus - Rodger A. Brown and Tetsuya Fujita

43. A Program for Computer Gridding of Satellite Photographs for Mesoscale Research - William D. Bonner

44. Comparison of Grassland Surface Temperatures Measured by TIROS VII and Airborne Radiometers under Clear Sky and Cirriform Cloud Conditions - Ronald M. Reap

45. Death Valley Temperature Analysis Utilizing Nimbus I Infrared Data and Ground-Based Measurements - Ronald M. Reap and Tetsuya Fujita

46. On the "Thunderstorm-High Controversy" - Rodger A. Brown

47. Application of Precise Fujita Method on Nimbus I Photo Gridding - Lt. Cmd. Ruben Nasta

48. A Proposed Method of Estimating Cloud-top Temperature, Cloud Cover, and Emissivity and Whiteness of Clouds from Short- and Long-wave Radiation Data Obtained by TIROS Scanning Radiometers - T. Fujita and H. Grandoso

49. Aerial Survey of the Palm Sunday Tornadoes of April 11, 1965 - Tetsuya Fujita

50. Early Stage of Tornado Development as Revealed by Satellite Photographs - Tetsuya Fujita

51. Features and Motions of Radar Echoes on Palm Sunday, 1965 - D. L. Bradbury and T. Fujita

52. Stability and Differential Advection Associated with Tornado Development - Tetsuya Fujita and Dorothy L. Bradbury

53. Estimated Wind Speeds of the Palm Sunday Tornadoes - Tetsuya Fujita

54. On the Determination of Exchange Coefficients: Part II - Rotating and Nonrotating Convective Currents - Rodger A. Brown

55. Satellite Meteorological Study of Evaporation and Cloud Formation over the Western Pacific under the Influence of the Winter Monsoon - K. Tsuchiya and T. Fujita

56. A Proposed Mechanism of Snowstorm Mesojet over Japan under the Influence of the Winter Monsoon - T. Fujita and K. Tsuchiya

57. Some Effects of Lake Michigan upon Squall Lines and Summertime Convection - Walter A. Lyons

58. Angular Dependence of Reflection from Stratiform Clouds as Measured by TIROS IV Scanning Radiometers - A. Rabbe

59. Use of Wet-beam Doppler Winds in the Determination of the Vertical Velocity of Raindrops inside Hurricane Rainbands - T. Fujita, P. Black and A. Loesch

60. A Model of Typhoons Accompanied by Inner and Outer Rainbands - Tetsuya Fujita, Tatsuo Izawa, Kazuo Watanabe and Ichiro Imai

61. Three-Dimensional Growth Characteristics of an Orographic Thunderstorm System - Rodger A. Brown

62. Split of a Thunderstorm into Anticyclonic and Cyclonic Storms and their Motion as Determined from Numerical Model Experiments - Tetsuya Fujita and Hector Grandoso

63. Preliminary Investigation of Peripheral Subsidence Associated with Hurricane Outflow - Ronald M. Reap

64. The Time Change of Cloud Features in Hurricane Anna, 1961, from the Easterly Wave Stage to Hurricane Dissipation - James E. Arnold

65. Easterly Wave Activity over Africa and in the Atlantic with a Note on the Intertropical Convergence Zone during Early July 1961 - James E. Arnold

66. Mesoscale Motions in Oceanic Stratus as Revealed by Satellite Data - Walter A. Lyons and Tetsuya Fujita

67. Mesoscale Aspects of Orographic Influences on Flow and Precipitation Patterns - Tetsuya Fujita

68. A Mesometeorological Study of a Subtropical Mesocyclone -Hidetoshi Arakawa, Kazuo Watanabe, Kiyoshi Tsuchiya and Tetsuya Fujita

69. Estimation of Tornado Wind Speed from Characteristic Ground Marks - Tetsuya Fujita, Dorothy L. Bradbury and Peter G. Black

70. Computation of Height and Velocity of Clouds from Dual, Whole-Sky, Time-Lapse Picture Sequences - Dorothy L. Bradbury and Tetsuya Fujita

71. A Study of Mesoscale Cloud Motions Computed from ATS-I and Terrestrial Photographs - Tetsuya Fujita, Dorothy L. Bradbury, Clifford Murino and Louis Hull

72. Aerial Measurement of Radiation Temperatures over Mt. Fuji and Tokyo Areas and Their Application to the Determination of Ground- and Water-Surface Temperatures - Tetsuya Fujita, Gisela Baralt and Kiyoshi Tsuchiya

73. Angular Dependence of Reflected Solar Radiation from Sahara Measured by TIROS VII in a Torquing Maneuver - Rene Mendez.

74. The Control of Summertime Cumuli and Thunderstorms by Lake Michigan During Non-Lake Breeze Conditions - Walter A. Lyons and John W. Wilson

75. Heavy Snow in the Chicago Area as Revealed by Satellite Pictures - James Bunting and Donna Lamb

76. A Model of Typhoons with Outflow and Subsidence Layers - Tatsuo Izawa

* out of print

(continued on outside back cover)

SATELLITE AND MESOMETEOROLOGY RESEARCH PROJECT --- PAPERS
(Continued from inside back cover)

77. Yaw Corrections for Accurate Gridding of Nimbus HRIR Data - Roland A. Madden.

78. Formation and Structure of Equatorial Anticyclones Caused by Large-Scale Cross Equatorial Flows Determined by ATS I Photographs - Tetsuya T. Fujita and Kazuo Watanabe and Tatsuo Izawa.

79. Determination of Mass Outflow from a Thunderstorm Complex Using ATS III Pictures - T. T. Fujita and D. L. Bradbury.

80. Development of a Dry Line as Shown by ATS Cloud Photography and Verified by Radar and Conventional Aerological Data - Dorothy L. Bradbury.

81. Dynamical Analysis of Outflow from Tornado-Producing Thunderstorms as Revealed by ATS III Pictures - K. Ninomiya.

82.** Computation of Cloud Heights from Shadow Positions through Single Image Photogrammetry of Apollo Pictures - T. T. Fujita.

83. Aircraft, Spacecraft, Satellite and Radar Observations of Hurricane Gladys, 1968 - R. Cecil Gentry, Tetsuya T. Fujita and Robert C. Sheets.

84. Basic Problems on Cloud Identification Related to the Design of SMS-GOES Spin Scan Radiometers - Tetsuya T. Fujita.

85. Mesoscale Modification of Synoptic Situations over the Area of Thunderstorms' Development as Revealed by ATS III and Aerological Data - K. Ninomiya.

86. Palm Sunday Tornadoes of April 11, 1965 - T. T. Fujita, Dorothy L. Bradbury and C. F. Van Thullenar (Reprint from Mon. Wea. Rev., 98, 29-69, 1970).

87. Patterns of Equivalent Blackbody Temperature and Reflectance of Model Clouds Computed by Changing Radiometer's Field of View - Jaime J. Tecson.

88. Lubbock Tornadoes of 11 May 1970 - Tetsuya Theodore Fujita.

89. Estimate of Areal Probability of Tornadoes from Inflationary Reporting of Their Frequencies - Tetsuya T. Fujita.

90. Application of ATS III Photographs for Determination of Dust and Cloud Velocities Over Northern Tropical Atlantic - Tetsuya T. Fujita.

91. A Proposed Characterization of Tornadoes and Hurricanes by Area and Intensity - Tetsuya T. Fujita.

92. Estimate of Maximum Wind Speeds of Tornadoes in Three Northwestern States - T. Theodore Fujita.

93. In- and Outflow Field of Hurricane Debbie as Revealed by Echo and Cloud Velocities from Airborne Radar and ATS-III Pictures - T. T. Fujita and P. G. Black (Reprinted from preprint of Radar Meteorology Conference, November 17-20, 1970, Tucson, Arizona).

94. Characterization of 1965 Tornadoes by their Area and Intensity - Jaime J. Tecson.

95.* Computation of Height and Velocity of Clouds over Barbados from a Whole-Sky Camera Network - Richard D. Lyons.

96. The Filling over Land of Hurricane Camille, August 17-18, 1969 - Dorothy L. Bradbury.

97. Tornado Occurrences Related to Overshooting Cloud-Top Heights as Determined from ATS Pictures - T. Theodore Fujita.

98. F P P Tornado Scale and its Applications - T. Theodore Fujita and A. D. Pearson.

99. Preliminary Results of Tornado Watch Experiment 1971 - T. T. Fujita, J. J. Tecson and L. A. Schaal.

100. F-Scale Classification of 1971 Tornadoes - T. Theodore Fujita.

101. Typhoon-Associated Tornadoes in Japan and New Evidence of Suction Vortices in a Tornado near Tokyo - T. Theodore Fujita.

102. Proposed Mechanism of Suction Spots Accompanied by Tornadoes - T. Theodore Fujita.

103. A Climatological Study of Cloud Formation over the Atlantic During Winter Monsoon - H. Shitara

104.** Statistical Analysis of 1971 Tornadoes - Edward W. Pearl.

105. Estimate of Maximum Windspeeds of Tornadoes in Southernmost Rockies - T. Theodore Fujita.

106. Use of ATS Pictures in Hurricane Modification - T. Theodore Fujita.

107. Mesoscale Analysis of Tropical Latin America - T. Theodore Fujita.

108. Tornadoes Around The World - T. Theodore Fujita. (Reprinted from Weatherwise, Vol.26, No. 2, April 1973)

109. A Study of Satellite-Observed Cloud Patterns of Tropical Cyclones - Ekundayo E. Balogun.

110. METRACOM System of Cloud-Velocity Determination from Geostationary Satellite Pictures - Yun-Mei Chang, Jaime J. Tecson and T. Theodore Fujita.

111. Proposed Mechanism of Tornado Formation from Rotating Thunderstorm - T. Theodore Fujita.

112. Joliet Tornado of April 6, 1972 - Edward W. Pearl.

113. Results of FPP Classification of 1971 and 1972 Tornadoes - T. T. Fujita and A. D. Pearson.

114. Satellite-Tracked Cumulus Velocities - T. T. Fujita, E. W. Pearl and W. E. Shenk.

115. General and Local Circulation of Mantle and Atmosphere toward Prediction of Earthquakes and Tornadoes, T. T. Fujita and Kazuya Fujita.

116. Cloud Motion Field of Hurricane Ginger during the Seeding Period as determined by the Metracom System, J. J. Tecson, Y.-M. Chang and T. T. Fujita.